FELDER, S., and CHANSON, H. (2018). "Air–Water Flow Patterns of Hydraulic Jumps on Uniform Beds Macroroughness." *Journal of Hydraulic Engineering*, ASCE, Vol. 144, No. 3, Paper 04017068, 12 pages (DOI: 10.1061/(ASCE)HY.1943-7900.0001402) (ISSN 0733-9429).

Air-water flow patterns of hydraulic jumps on uniform bed macro-roughness

Stefan Felder[1] and Hubert Chanson[2]

Abstract: Hydraulic jumps are characterised by strong flow turbulence, flow aeration and three-dimensional flow motions. While comprehensive research into hydraulic jumps on smooth bed has improved the understanding of flow aeration and turbulence, limited research has been done of hydraulic jumps on rough bed. Herein novel experiments were conducted in hydraulic jumps on uniformly-distributed bed macro-roughness. Both air-water flow patterns and basic air-water flow properties were investigated. The hydraulic jumps on the rough bed exhibited some remarkable differences compared to smooth bed jumps including some pre-aeration of the flow upstream of the jump, an upwards shift of the jump roller and a clear water flow region underneath the jump. Air-water flow measurements were conducted with a phase-detection probe, showing similar distributions of air-water flow properties for the rough and smooth bed jumps. Comparative analyses highlighted some distinctive effects of the bed roughness including an upwards shift of the hydraulic jump and an increase in bubble count rate and void fractions in the region close to the jump toe. In the second half of the hydraulic jumps the rough bed led to a clear water region with large scale vortices which were advected downstream. The present study highlighted the potential that improved and non-standard invert designs may have for flow manipulations and design enhancements.

Keywords: Hydraulic jump; bed macro-roughness; conjugate depth; flow patterns; air-water flows

Introduction

Hydraulic jumps occur in many natural waterways, open channels and canals as well as downstream of man-made hydraulic structures when fast flowing supercritical flow transitions into subcritical flows (Bélanger 1841; Bakhmeteff 1932). The transition is sudden, extremely turbulent and associated with energy dissipation, air entrainment, large-scale turbulence, spray, splashing, and surface waves. A hydraulic jump is a strong dissipative process commonly observed in stilling basins (Hager 1992; Chanson and Carvalho 2015). The flow turbulence is extremely complicated and three-dimensional in the jump roller (Liu et al. 2004; Lennon and Hill 2006; Wang and Chanson 2015), and it remains a challenge to engineers, scientists and researchers (Rajaratnam 1967; Chanson 2009). Basic features of jumps with a breaking roller are the development of large-scale vortices, the air bubble entrapment at the jump toe, the interfacial aeration/de-aeration at the roller upper free-surface and the interactions between entrained bubbles and coherent turbulent structures in the jump roller (Rouse et al. 1959; Resch and Leutheusser 1972; Babb and Aus 1981; Zhang et al. 2014; Wang et al. 2014).

The effects of bed roughness on hydraulic jumps were investigated (a) in terms of the impact of baffles in stilling basins and (b) with uniformly distributed roughness (Table 1). Hydraulic jump stilling basins are relatively expensive structures, and detailed hydraulic design guidelines were developed based upon extensive physical modelling (e.g. Bradley and Peterka 1957). The design may include steps, blocks, baffles, sills, expansion, drops, typically used to increase the rate of energy dissipation, decrease the basin length and stabilise the jump toe position (USBR 1987; Chanson and Carvalho 2015).

A number of physical studies have been conducted on hydraulic jumps above uniformly distributed roughness (Table 1). Table 1 summarises key parameters of most relevant studies of hydraulic jumps on rough channel bed, including the equivalent sand roughness height k_s, channel width B, conjugate depth upstream of the hydraulic jump d_1, upstream Froude number $Fr_1 = V/(g \times d_1)^{0.5}$, Reynolds number Re and the water discharge Q_w. Following Rajaratnam (1968), and Leutheusser and Schiller

(1975), most investigations focused on simple free-surface measurements to identify the conjugate depth relationship for hydraulic jumps on rough channel beds. A few studies incorporated measurements with Pitot tubes to measure the mean velocity distributions and boundary layer parameters in the mono-phase flow region of the jump (Table 1). Recently Pagliara and Palermo (2015) used a single-tip conductivity probe to measure the conjugate depth taking into account any pre-aeration effect upstream of the jump and flow aeration downstream of the jump. While this study highlighted the relevance of aeration on the conjugate depth relationship, no study documented the bed roughness effects on the air-water flows in hydraulic jumps. Herein, this manuscript presents comprehensive observations of basic air-water flow patterns and air-water flow properties in hydraulic jumps on uniformly distributed macro-channel bed roughness (Table 1).

Experimental facility and flow configurations

Experiments were conducted in a flume with rectangular test section of 3.2 m length, 0.5 m width and 0.41 m height. The flume consisted of a horizontal high-density polyethylene (HDPE) bed and glass sidewalls. A constant flow rate was supplied from an upstream header tank through a vertical sluice gate equipped with a rounding (Ø = 0.3 m) (Fig. 1). At the downstream end of the flume, an adjustable sharp-crested weir controlled the location of the hydraulic jump. In the present experiments, the jump toe position was located at x_1 = 1 m downstream of the sluice gate for all flow conditions. The distance x_1 = 1 m was selected for consistency and comparison with previous experiments of hydraulic jumps on smooth bed in the same channel (e.g. Chachereau and Chanson 2011; Wang 2014; Wang et al. 2014). Further details about the setup of the flume can be found in Wang (2014), Wang and Chanson (2015) and Felder and Chanson (2016a).

The flow rate was measured with a Venturi flow meter in the supply pipe. Experiments were conducted for a range of discharges $0.012 < Q_w < 0.106$ m^3/s, for three sluice gate openings (h = 20 mm, 36 mm & 52 mm), for Reynolds numbers $3.3\times10^4 < Re < 1.5\times10^5$ and upstream Froude numbers $1.5 < Fr_1 < 6.5$. All present flow conditions are listed in Table 1. Note that the upstream flow was rough and aerated for several flow conditions affecting the accuracy of the flow depth recording and that the upstream depth d_1 was defined in terms of the equivalent clear-water depth d determined based upon void fraction measurements:

$$d = \int_{y=0}^{Y_{90}} (1 - C) \times dy \quad (1)$$

where C is the local void fraction, y the vertical elevation of the measurement position and Y_{90} the characteristic flow depth where C = 0.9.

The roughness effects on hydraulic jumps were tested using three different bed roughness configurations. The first configuration was the reference configuration with smooth channel bed, a configuration extensively researched in recent years (Murzyn and Chanson 2008; Chachereau and Chanson 2011; Wang 2014). The rough bed setups comprised two different bed roughness configurations consisting of industrial rubber mats installed over the full length of the channel including upstream of and underneath the sluice gate (Fig. 1). In rough bed configuration 1, the rubber mats were installed conventionally leaving some small continuous gaps between the HDPE invert and rubber mat floor (Fig. 1A). The total thickness of the rubber mat from the HDPE bed to the top of the mat was 25.5 mm. The top of the rubber mat was defined as the zero position for the vertical elevations and visual observations of air bubbles within the flow confirmed negligible contribution of the underlying gaps to the overall flow rate, while recirculating motions indicated that the holes in the rubber mat contributed to the overall flow resistance. In rough bed configuration 2, the rubber mats were placed upside down creating a regular pattern of larger roughness elements (Fig. 1B). The

vertical zero position was defined below the spikes on the horizontal and vertical strips positioned 17.7 mm above the smooth HDPE bed. The rubber mat configurations were previously used by Leng and Chanson (2015) who quantified the roughness characteristics during detailed open channel flow experiments resulting in an average equivalent sand roughness height of k_s = 12 mm for roughness configuration 1 and of k_s = 39 mm for configuration 2. These data were obtained in subcritical gradually varied steady flow conditions. It is acknowledged that the present experiments were conducted under supercritical flow conditions and that the equivalent sand roughness height might differ from the reported values. While the roughness of the rubber mats was uniformly distributed, the shapes of the roughness were quite specific with small voids underneath the rubber mat for rough bed 1 and protruding spikes for rough bed 2. These specific roughness features contributed to the overall flow resistance, and flow depth, and the use of the equivalent sand roughness appeared to be a reasonable roughness estimate, allowing a direct comparison with other rough bed elements. The definition of the zero position (y = 0) was carefully selected based upon flow observations and considerations of most suitable zero elevation. For rough bed 1, the zero position was therefore located at the top of the rubber mat and for rough bed 2, at the top of the vertical cross-strips. These zero positions appeared most meaningful and it is acknowledged that changes in the definition of the zero position could lead to differences in flow depth. This is particularly the case for rough bed 2 where the protruding spikes could have shifted the zero position upwards resulting in a reduction of the flow depth. Further details about the channel bed roughness can be found in Leng and Chanson (2015) and Felder and Chanson (2016a).

Air-water flow experiments were conducted with a dual-tip conductivity probe manufactured at the UNSW Water Research Laboratory. The conductivity probe consisted of identical leading and trailing tips with needle sensors made of an inner Platinum wire (Ø = 0.125 mm) and insulated from the outer electrode made of a metal tube (Ø = 0.5 mm). The leading and trailing tips were separated in longitudinal and transverse directions by Δx = 7.9 mm and Δz = 1.0 mm respectively. The leading tip was positioned in channel centre line parallel to the flow direction and the trailing tip was positioned at the same vertical elevation. The sensors were initially positioned immediately above the channel bed for the respective roughness configuration and shifted vertically with a Mitutoyo™ digimatic scale for profiling of air-water flow properties within a cross-section. Both probe sensors were sampled simultaneously for 45 s at 20 kHz following Felder and Chanson (2015). The recorded raw signals were post-processed with a Fortran code (Felder 2013) to calculate the time averaged local void fraction C and the local bubble count rate F based upon a single threshold of 50%, as well as the local time-averaged interfacial velocity V based upon a cross-correlation of the two tip signals.

In addition a pointer gauge was used to record non-aerated flow depths upstream and downstream of the hydraulic jump. Detailed documentation of the flow patterns was conducted with SLR digital cameras Canon™ DOS 450D and Pentax™ K-3 as well as video camera Sony™ Handycam HDR-CW100E and a digital camera Casio™ Exilim EX-10 with high-speed video capabilities. Further details were reported in Felder and Chanson (2016a).

Basic air-water flow patterns

Flow patterns of hydraulic jumps with bed roughness 1

For rough bed configuration 1, the flow patterns exhibited four different hydraulic jump types, comprising undular jumps, undular jumps with air entrainment, hydraulic jumps with small roller and wavy surface downstream and hydraulic jumps with distinct jump toe roller (Fig. 2). For all investigated flow conditions, the free-surface was rough in both super- and sub-critical flow regions. The free-surface roughness was particularly observed for flow conditions with small flow depths such as the supercritical flow region between sluice gate and jump toe as well as for the undular jumps along the full length of the channel.

For Froude numbers $Fr_1 \leq 2.2$, undular jumps were observed independently of the gate opening (Fig. 2A). Such a range of Froude numbers was slightly larger compared to smooth bed undular jumps

(Montes and Chanson 1998; Reinauer and Hager 1995), although the upper limit of undular jumps is related to the aspect ratio d_c/B, where d_c is the critical flow depth (Montes and Chanson 1998). The flow patterns showed three dimensional free-surface profiles with instable undulations, oscillating in both longitudinal and transverse directions. Within the central section of the undular jump, distinct standing waves were observed with several troughs and peaks (Fig. 2A). With decreasing inflow depth (i.e. smaller gate openings), these undulations were less distinguishable and the free-surface ripples buffered the undulations. The longitudinal free-surface profiles of the undular jumps as well as the wave length and the wave amplitude between first and second crest of the undular jumps were recorded with a pointer gauge. The observations showed decay in wave length with increasing Froude numbers independent of the bed roughness and smaller wave amplitudes for the rough bed compared to previous observations on smooth bed. Smaller wave amplitudes suggested that the bed roughness contributed to some energy dissipation.

For $2.2 < Fr_1 \leq 2.6$, undular jumps with air entrainment were observed (Fig. 2B). These jumps were similar in appearance to the non-aerated undular jumps, albeit with stronger free-surface fluctuations and standing waves. A key difference was the entrainment of air at the first undular wave crest downstream of the jump toe and to a smaller extent at the following wave crests. The entrained air consisted of clearly distinguishable bubbles being transported downstream before rising to the free-surface. In addition some small white capping was observed at the surface of the first wave crest and to a lesser extent at following wave crests in channel centreline (Fig. 2B). The air entrainment process and the formation of surface air caps were not stationary and were linked to the fluctuating motion of the undular jumps and the three dimensional flow features.

With increasing Froude number, a roller formed at the jump toe and, for $2.7 \leq Fr_1 \leq 2.9$, the roller formation at the jump toe was unstable resulting in secondary undulations of the free-surface further downstream (Fig. 2C). The jump flow was affected by the upstream flow depth resulting in less stable roller formation for the smallest gate opening.

For $Fr_1 \geq 3.0$, the hydraulic jump had a marked roller with strong turbulence downstream of the jump toe (Fig. 2D). Upstream of the jump, the supercritical inflow was characterised by strong free-surface roughness which increased with decreasing flow depth and gate height. For the smallest gate opening ($h = 20$ mm), the flow became pre-aerated for the largest flow rates ($Q_w > 0.035$ m^3/s; $Fr_1 > 3.3$). Although the overall appearance of the jumps with stable roller was similar to hydraulic jumps on smooth bed, a distinctive difference was associated with large-scale vortical structures downstream of the jump toe. For the two largest gate openings, the jump toe was shifted towards the surface resulting in a clear water flow region below the jump roller (Fig. 2D). With increasing gate opening and flow depth respectively, the clear water flow region height increased. The presence of a clear water flow region resulted in a very distinctive vortex street formation downstream of the jump toe, with periodic air bubble vortex shedding into the clear water core region under the jump (Fig. 2D). The interactions between the clear water boundary layer and the vortex shedding led to the formation of large scale eddies within the flow consisting of tubelike vortical structures that were advected downstream. These structures were visible in the aerated roller region (Fig. 2D). These large scale vortical structures were also observed in the hydraulic jump with smallest gate opening ($h = 20$ mm), although the clear water core region beneath the jump roller was small and the vortex street formation was subdued. Little visible difference was observed in terms of free-surface flow patterns, characterised by strong splashing at the jump toe and irregular surface fluctuations further downstream. Further documentation of the flow patterns can be found in Felder and Chanson (2016a).

Jump toe perimeter characteristics on bed roughness 1

For hydraulic jumps with stable jump toe roller on bed roughness 1, the jump toe fluctuated in the longitudinal direction, in a manner similar to known features of hydraulic jumps on smooth bed (e.g. Long et al. 1991, Chachereau and Chanson 2011; Wang 2014). A detailed investigation of the jump toe positions was conducted to identify the effect of bed roughness upon the jump toe perimeter

properties. The jump toe perimeter characterised the longitudinal position of the roller toe location at several transverse positions z across the channel. For three hydraulic jumps on rough bed 1 and for the smooth bed hydraulic jump, videos of the jump toe perimeters were recorded for 1 minute from above and 600 images of hydraulic perimeters were analysed for each hydraulic jump, with a minimum of 100 perimeter points per image. The results provided the average jump toe perimeter position x_{toe}, the standard deviation of the jump toe position x_{toe}' and the differences in 10^{th} and 90^{th} percentile of the jump toe position (x_{90}-x_{10}) (Fig. 3).

The results highlighted some difference between rough and smooth bed hydraulic jump toe perimeters. While the smooth bed data were consistent with earlier observations by Wang (2014), the rough bed data did not show a clear trend. The mean perimeter profiles were relatively close for all investigated hydraulic jumps (Fig. 3A). The mean profiles for all hydraulic jumps herein showed roller toe perimeters relatively close to the mean jump toe position independently of the bed roughness. With increasing transverse distance from the channel centreline, the jump toe was on average upstream of the mean jump toe position, irrespective of the bed roughness (Fig. 3A). Large differences were found in terms of the standard deviation with a large spread of values for the three rough bed hydraulic jumps (Fig. 3B). While Wang (2014) reported an increase of standard deviation on smooth bed jumps with increasing Froude number, the rough bed jump with $Fr_1 = 5.5$ exhibited the strongest standard deviation. In contrast the observations of the differences in 90^{th} and 10^{th} percentile showed a closer agreement of the hydraulic jumps with comparable Froude numbers independent of the bed roughness (Fig. 3C).

The hydraulic jump with $Fr_1 = 5.5$ was characterised by fast fluctuations of the jump toe perimeter and the oscillatory movement of the jump toe was in agreement with the higher Froude number jumps. For the rough bed jump with largest inflow depth, and smallest relative roughness, and smallest Froude number, both standard deviation and differences in percentiles were smallest which was consistent with observations on smooth bed (Wang 2014). Overall, the present observations suggested that the hydraulic jumps on the rough bed did not follow a clear trend in terms of inflow Froude number, although the bed roughness had some effect upon the hydraulic jump toe fluctuations.

Flow patterns of hydraulic jumps with bed roughness 2

The flow patterns of hydraulic jumps on rough bed configuration 2 showed some distinctive features, not observed on smooth bed jumps (Fig. 4). Upstream of the jump, the free-surface in the inflow region was characterised by strong free-surface roughness reflecting the macro-roughness of the channel bed. In comparison with rough bed configuration 1, the free-surface roughness was more pronounced both upstream and downstream of the jump toe. For all gate openings, the upstream flow became aerated for the largest flow rates. With decreasing flow depth and gate opening, pre-aeration was also present for much smaller flow conditions (Fig. 4). The pre-aeration of the inflow allowed some visualisation of the upstream flow, highlighting recirculation movements within the spaces between the large rough elements and sudden cavity ejections. These observations highlighted the momentum exchange processes close to the rough bed and the overlying free-stream flows. The large roughness of the channel bed led to a rapid growth of the turbulent boundary layer immediately downstream of the sluice gate. While the boundary layer development was not measured in the present study, it is assumed that the air entrainment started naturally when the boundary layer outer edge reached the free-surface, in a fashion similar to spillway flows (Wood et al. 1983; Felder and Chanson 2014). This self-entrainment process is typically linked to strong turbulence fluctuations close to the free-surface overcoming both surface tension and buoyancy effects. In the present study, the inception of the free-surface aeration started earlier with decreasing flow depth and increasing flow velocity, which is consistent with the onset of free-surface aeration in self-aerated high-velocity free-surface flows on spillways.

Four types of hydraulic jump flows were observed for rough bed configuration 2 comprising undular jumps with flow aeration, hydraulic jumps with standing wave, hydraulic jumps with distinct roller

and oscillating jumps between the latter two jump types. For inflow Froude numbers $Fr_1 < 2.3$, an undular hydraulic jump was observed with air entrainment at the first wave crest (Fig. 4A). While the flow was pre-aerated for the smallest gate opening, for the larger gate openings no pre-aeration was observed. The undular flow patterns was three dimensional with some instable fluctuations of the free-surface and pseudo-periodic appearance of troughs and peaks. The undular jump free-surface appeared much rougher compared to both undular jumps on smooth bed and on rough bed configuration 1.

For $2.3 \leq Fr_1 < 3$, a hydraulic jump with standing wave at the jump toe developed resulting in air entrainment at the start of the jump and some significant free-surface waves downstream (Fig. 4B). No distinct jump toe or jump toe location was observed and some longitudinal fluctuations were present. The standing wave was not stable resulting in unsteady jump waves further downstream and significant free-surface fluctuations downstream of the standing wave as well as fluctuations of the free-surface before the downstream gate. The flow appearance was similar to the type of non-developed hydraulic jump reported by Carollo et al. (2007). The flow was aerated at the standing wave for the largest gate openings, and pre-aerated for the smallest gate opening.

For a Froude number $Fr_1 \approx 3$, the hydraulic jump oscillated between a hydraulic jump with standing wave and a hydraulic jump with distinct roller. The oscillation occurred periodically with a period of more than one minute. Such an oscillating jump was characterised by movement of the jump toe in longitudinal direction which resulted in the change of flow patterns between the two different jump types. The oscillations were similar to the observations by Mossa (1999) who observed oscillating jumps in channels with abrupt drop in bed height and an irregular natural channel profile. The oscillations were also similar to the pulsating flow movement at the upstream end of a mild sloped pooled stepped spillway, reported by Felder and Chanson (2013). Figure 4C illustrates the oscillating jump highlighting the change-over from the standing wave jump to the roller jump. The oscillating jump occurred for the gate openings of h = 36 & 52 mm and was not observed for the smallest gate opening suggesting that the inflow conditions played a role in the jump oscillations.

For Froude numbers $Fr_1 > 3$, hydraulic jumps with marked roller and well-defined jump toe were observed. The inflow was pre-aerated for all gate openings (Fig. 4D). While the appearance of the jump toe and the free-surface was similar to hydraulic jumps on smooth channel bed as well as rough bed configuration 1, the flow structure beneath the free-surface showed some marked differences. The jump appeared more aerated in the shear region close to the jump toe; this might be linked with the pre-aeration of the inflow. The bed roughness increased the shear stress and the more violent motion of the free-surface led to entrapment of air from above. The jump roller appeared shorter and showed some upward motion. The vortex shedding appeared to be affected by the bed roughness leading to much less pronounced shedding. A clear feature was the large scale vortical structures which developed downstream of the jump roller and were advected downstream without losing their momentum. For the largest gate openings, a small clear water flow region was observed beneath the shear region expanding to a region without any air entrainment further downstream. The existence of such a clear water flow region was consistent with the upward roller motion at the jump toe. Overall the appearance of the hydraulic jump with roller was markedly different to hydraulic jumps on smooth bed. Herein the current experiments were limited to a maximum upstream Froude number of $Fr_1 = 4.3$, for the largest gate opening. Larger inflow conditions would result in stronger pre-aeration of the flow impacting further upon the hydraulic jump characteristics.

Free-surface characteristics

A hydraulic jump constitutes some form of discontinuity in terms of the pressure and velocity fields at the jump toe. In an integral form, the continuity and momentum principles give a system of equations linking the flow properties upstream and downstream of the jump (Lighthill 1978). For a horizontal channel with prismatic rectangular cross-section, the solution of the momentum and continuity equations yields (Chanson 2012):

$$Fr_1^2 = \frac{1}{2} \times \frac{d_2}{d_1} \times \left(\left(1 + \frac{d_2}{d_1}\right) + \frac{1}{\frac{d_2}{d_1} - 1} \times \frac{F_{fric}}{\rho \times g \times B \times d_1^2} \right) \quad (2)$$

Equation (2) expresses the upstream Froude number as a function of the ratio of conjugate depths d_2/d_1 and the flow resistance force F_{fric}. For a fixed upstream Froude number, the effects of bed friction implies a smaller ratio of conjugate depths d_2/d_1 with increasing flow resistance. The finding is consistent with physical data in laboratory flumes (Leutheusser and Schiller 1975; Pagliara et al. 2008). In the case of a smooth horizontal rectangular prismatic channel ($F_{Fric} \approx 0$), Equation (2) may be simplified into the classical Bélanger equation (Bélanger 1841):

$$\frac{d_2}{d_1} = \frac{1}{2} \times \left(\sqrt{1 + 8 \times Fr_1^2} - 1 \right) \quad (3)$$

For all flow configurations (Table 1), the conjugate depth relationship was recorded. The upstream conjugate depth was measured slightly upstream of the jump toe at $x_1 = 0.85$ m and the subcritical conjugate depth at the downstream end of the channel ($x_2 = 2.8$ m). The experimental data for the two rough bed configurations are presented in Figure 5. The data combine both pointer gauge data (hollow symbols) and air-water flow data (solid symbols). For the rough channel bed, both free-surface roughness and air entrainment led to some inaccuracy in terms of the upstream flow depth measurements with a pointer gauge. Therefore the upstream flow depth d_1 was adjusted against the average equivalent clear water flow depth d (Eq. (1)). The downstream flow depth was always recorded with the pointer gauge since the effect of the aeration was small and the surface roughness was minimal on the larger flow depth.

Figure 5 shows a clear trend in terms of conjugate depth ratio; the rough bed data are located below the Bélanger equation, valid only for smooth frictionless rectangular horizontal channels (Eq. (3)). All present data were however above the results of Ead and Rajaratnam (2002) for hydraulic jumps on corrugated channels. The observed conjugate depth data were consistent with theoretical predictions (Eq. (2)), indicating a loss of momentum through friction effects on the channel bed for both rough bed configurations. The data were overall in agreement with previous studies of roughness effects (e.g. Hughes and Flack 1984; Carollo et al. 2007; Afzal et al. 2011; Pagliara and Palermo 2015). The present data for the two rough bed configurations were in good agreement and no downwards shift of the conjugate depth relationship was observed for rough bed 2. This finding differed from previous studies, showing a downward shift of conjugate depth ratio with increasing equivalent sand roughness height (e.g. Carollo et al. 2007; Afzal et al. 2011; Pagliara and Palermo 2015). It is believed that the exact definition of d_1 may have had an impact upon the conjugate depth relationship: i.e., specifically the measurement of the free-surface with a pointer gauge in previous studies and possibly the definition of the zero position in rough bed 2 in the present study.

Based upon momentum considerations for a rectangular horizontal channel (Eq. (2)), an expression of the boundary shear force F_{frict} may be derived as a function of the ratio of conjugate depths and inflow Froude number:

$$\frac{F_{fric}}{\rho \times g \times B \times d_1^2} = \left(\frac{Fr_1^2}{\frac{1}{2} \times \frac{d_2}{d_1}} - \left(1 + \frac{d_2}{d_1}\right) \right) \times \left(\frac{d_2}{d_1} - 1 \right) \quad (4)$$

Assuming that the roller length is about $L_r/d_1 = 6\times(Fr_1-1)$ (Wang 2014), the average boundary shear stress τ_o beneath the roller equals:

$$\frac{\tau_o}{\frac{1}{2}\times\rho\times V_1^2} = \frac{\left(\frac{d_2}{d_1}-1\right)}{3\times Fr_1^2\times(Fr_1-1)}\times\left(\frac{Fr_1^2}{\frac{1}{2}\times\frac{d_2}{d_1}}-\left(1+\frac{d_2}{d_1}\right)\right) \quad (5)$$

The boundary friction force and average boundary shear stress were estimated based upon the observed ratios of conjugate depths and inflow Froude numbers using Equations (4) and (5) respectively. The results are presented in Figure 6. The dimensionless data showed some correlation in terms of Reynolds number Re and equivalent roughness height (Fig. 6B). Namely the dimensionless shear stress decreased exponentially with increasing Reynolds number:

$$\frac{\tau_o}{\frac{1}{2}\times\rho\times V_1^2} = a\times e^{-b\times Re} \quad (6)$$

For a given Reynolds number and inflow depth, the dimensionless boundary shear stress was larger for the rougher bed configuration 2.

Air-water flow properties

For selected flow conditions, air-water flow measurements were conducted with the double-tip conductivity probe yielding void fraction, bubble count rate and interfacial velocity distributions for the two rough and smooth bed configurations (Table 1). Typical distributions are presented in Figure 7, showing key features of the air-water flow properties within hydraulic jumps on macro roughness, as functions of the dimensionless elevation above channel bed y/d_1 (Fig. 7). Note that the overall air-water flow properties are little affected by the exact definition of the zero position (see above) and the comparative analysis and the overall findings may be used as general guide for hydraulic jumps on rough bed. The results are presented for comparable Froude and Reynolds numbers and for similar cross-sections within the hydraulic jump.

Figure 7A presents typical void fraction distributions highlighting a few key differences between the two rough bed configurations and smooth bed jump data. All void fraction distributions had similar shapes independently of the bed roughness. In the turbulent shear region, a local maximum void fraction was observed, while a local minimum was found at the boundary between the shear region and the upper free-surface region where recirculation took place. Close to the channel bed, the void fraction tended to zero. In the upper free-surface region the void fraction increased sharply with increasing elevation towards unity (Fig. 7A).

Although the shape of void fraction distributions was similar, a number of differences were observed. Immediately downstream of the jump toe, the void fraction distributions for rough bed 1 and the smooth bed were quite similar, while the distributions on rough bed 2 showed slightly smaller void fraction values as well as an upward shift. Further downstream, the differences increased between the three configurations. While the void fraction distributions on smooth bed were consistent with previous experimental observations showing both turbulent shear and recirculation regions, the distributions for the rough bed differed. For the rough bed, the shear region was shifted upwards and no recirculation region was observed towards the downstream end. While the elevation of maximum void fraction in the shear region was similar close to the jump toe for the rough and smooth bed configurations, the elevations of maximum void fractions differed towards the downstream end of the hydraulic jump. With increasing bed roughness, the upward shift of the shear region increased (Fig. 7A). The data confirmed the visual observation of an upward directed roller for the rough bed configurations. Detailed assessment of scale effects showed that the void fraction observations were

independent of scale effects (Felder and Chanson 2016a), as previously reported for comparable hydraulicn jump flows on smooth bed (Chanson and Gualtieri 2008, Murzyn and Chanson 2008).
The bubble count rate distributions revealed distinct effects of channel bed roughness (Fig. 7B). The bubble count rate is affected by significant scale effects and the number of entrained air bubbles cannot be scaled based solely upon a Froude similitude (Murzyn and Chanson 2008, Chanson and Chachereau 2013). While the data are compared for similar Froude and Reynolds numbers (Fig. 7B), it is acknowledged that the present analysis did not achieve exact similitude in terms of both Froude and Reynolds numbers, but that the comparison provided valuable information about differences in bubble count rates between different channel bed roughness. In the first part of the jump roller, the bubble count rate in the shear region was significantly larger on rough bed 2 compared to the other two bed configurations which were in relatively close agreement. Such a larger bubble count rate might be linked with the pre-aeration of the upstream flow. Further downstream, the magnitude of the bubble count rate was similar for all bed roughness configurations. However distinct differences were observed in terms of the elevation of the maximum bubble count rate in a cross-section. While the elevations of maximum bubble count rate were similar at the start of the jump, the elevation of was shifted upwards towards the downstream end of the hydraulic jump. It appeared that the location of the shear region was shifted upwards with increasing bed roughness. This observation was consistent with the upward directed roller and the clear water flow region underneath the hydraulic jumps on rough bed, as well as with the observations of an upward shift in void fraction distributions.
The comparative results in terms of interfacial velocity distributions are presented in Figure 7C for similar Froude and Reynolds numbers. The interfacial velocity profiles exhibited similar features to void fraction and bubble count rate distributions, confirming an upward directed roller on the rough bed and a reduction in recirculation region towards the downstream end. Close to the jump toe the interfacial velocity distributions were overall similar (Fig. 7C). Further downstream however, the interfacial velocities became more uniform with increasing bed roughness and no recirculation region was observed towards the downstream end of the hydraulic jump. The finding suggested that the bed roughness enhanced the vertical momentum mixing, enabling the rapid development of a quasi-uniform velocity profile, typically observed downstream of hydraulic jumps with breaking roller (Wu and Rajaratnam 1996). The interfacial velocity distributions were not affected by scale effects (Felder and Chanson 2016a). Further details about the air-water flow properties can be found in Felder and Chanson (2016a, b).

Conclusion

An experimental study of hydraulic jumps on uniformly distributed macro-roughness was conducted at laboratory scale for a range of flow conditions ($1.5 < Fr_1 < 6.5$; $3.3 \times 10^4 < Re < 2.1 \times 10^5$). The experiments comprised three different bed configurations including smooth and two rough beds. Detailed observations of the flow patterns were conducted for the rough bed configurations revealing distinctive differences between smooth and rough bed jumps. For all flow conditions, the flow was three dimensional throughout the test section with large scale vortices being created in interactions of boundary layer on rough bed and vortex shedding processes behind the jump toe. An increase in bed roughness resulted in an increase in differences between rough and smooth bed configurations including a pre-aeration of the flow upstream of the hydraulic jump, an upwards shift of the jump roller and a clear water flow region underneath the jump. The visual observations highlighted a range of hydraulic jump types including undular jumps, stable jumps with rollers as well as jumps with standing waves and a cyclic transformation between roller jump and wave jump. While basic observations of the conjugate depth relationship confirmed the effect of flow resistance of the rough bed, the visual observations of flow patterns highlighted the strong effect of channel bed roughness upon the hydraulic jumps.

Basic distributions of air-water flow properties were measured with a phase-detection probe. While the distributions were overall similar for the rough and smooth bed hydraulic jumps, the comparative

analysis highlighted some distinctive effects upon the air-water flow properties with increasing bed roughness. The differences included an increase in bubble count rate and void fractions in the region close to the jump toe. In the second half of the jumps the rough bed led to elevated levels of void fraction in the recirculation region suggesting a lesser aeration of the free-surface region.

Overall the present study highlighted the effects of macro-roughness upon hydraulic jumps, showing the potential to manipulate hydraulic jump flow motion with the introduction of uniformly distributed roughness elements on the invert. The introduction of macro-roughness may be a suitable way to increase flow aeration and bubble break-up, which can be useful for industrial applications where air-water mass transfer processes and mixing processes are important. The introduction of uniformly distributed macro-roughness may have additional benefits including the dissipation of flow energy as the observations of the conjugate depth relationships suggested. The present study highlighted the potential that improved and non-standard designs may have for flow manipulations and design enhancements.

Acknowledgements
The authors thank Dr Hang Wang, Jason Van Der Gevel and Stewart Matthews (The University of Queensland) for their assistance in laboratory work. The authors thank Rob Jenkins (WRL, UNSW Australia) for manufacturing of the conductivity probe. The image analysis of jump toe perimeters was conducted by Preshit Wazalwar (IIT Bombay, India) as part of his undergraduate internship at WRL.

Notation

B	channel width (m)
C	void fraction
d	equivalent clear-water depth (m)
d_c	critical flow depth (m)
d_1	conjugate depth upstream of hydraulic jump (m)
d_2	conjugate depth downstream of hydraulic jump (m)
F	bubble count rate (Hz)
F_{fric}	Flow resistance force (N)
Fr_1	upstream Froude number
g	gravity acceleration constant (m/s^2);
h	sluice gate opening (m)
k_s	equivalent sand roughness (m);
Q_w	Water discharge (m^3/s);
Re	Reynolds number
V	Interfacial velocity (m/s)
V_1	Depth-average velocity upstream of hydraulic jump (m/s)
x_1	jump toe position (m)
x_{toe}	jump toe perimeter position (m)
x_{toe}'	standard deviation of jump toe perimeter position (m)
y	direction normal to flow direction
Y_{90}	flow depth where C = 0.9
z	transverse direction (m) across the channel, measured from the channel centreline
Δx	longitudinal distance between sensor tips (m)
Δz	transverse distance between sensor tips (m)
ρ	density (kg/m^3)
τ_o	shear stress (Pa)
Ø	diameter (m)

FELDER, S., and CHANSON, H. (2018). "Air–Water Flow Patterns of Hydraulic Jumps on Uniform Beds Macroroughness." *Journal of Hydraulic Engineering*, ASCE, Vol. 144, No. 3, Paper 04017068, 12 pages (DOI: 10.1061/(ASCE)HY.1943-7900.0001402) (ISSN 0733-9429).

References

Afzal, N., Bushra, A., Seena, A. (2011). "Analysis of Turbulent Hydraulic Jump over a Transitional Rough Bed of a Rectangular Channel: Universal Relations." J. Hydraul. Eng., 137, 835-845.

Babb, A.F., Aus, H.C. (1981). "Measurements of Air in Flowing Water." Jl of Hyd. Div., 107(HY12), 1615-1630.

Bakhmeteff, B.A. (1932). "Hydraulics of Open Channels." McGraw-Hill, New York, USA, 1st edition, 329 pages.

Bélanger, J.B. (1841). "Notes sur l'Hydraulique." ("Notes on Hydraulic Engineering.") Ecole Royale des Ponts et Chaussées, Paris, France, session 1841-1842, 223 pages (in French).

Bradley, J.N., Peterka, A.J. (1957). "The Hydraulic Design of Stilling Basins: Hydraulic Jumps on a Horizontal Apron (Basin I)." Jl of Hyd. Div., 83(HY5), 1401-1/1401-22.

Carollo, F.G., Ferro, V., Pampalone, V. (2007). "Hydraulic jump on rough beds." J. Hydraul. Eng., 133(9), 989–999.

Chachereau, Y., Chanson, H. (2011). "Free-Surface Fluctuations and Turbulence in Hydraulic Jumps." Experimental Thermal and Fluid Science, 35(6), 896-909 (DOI: 10.1016/j.expthermflusci.2011.01.009).

Chanson, H. (2009). "Current Knowledge In Hydraulic Jumps And Related Phenomena. A Survey of Experimental Results." European Journal of Mechanics B/Fluids, 28(2), 191-210 (DOI: 10.1016/j.euromechflu.2008.06.004).

Chanson, H. (2012). "Momentum Considerations in Hydraulic Jumps and Bores." Journal of Irrigation and Drainage Engineering, 138(4), 382-385 (DOI 10.1061/(ASCE)IR.1943-4774.0000409).

Chanson, H., Carvalho, R. (2015). "Hydraulic jumps and stilling basins." in "Energy Dissipation in Hydraulic Structures." IAHR Monograph, CRC Press, Taylor & Francis Group, Leiden, The Netherlands, 65-104.

Chanson, H., Chachereau, Y. (2013). "Scale Effects Affecting Two-Phase Flow Properties in Hydraulic Jump with Small Inflow Froude Number." Experimental Thermal and Fluid Science, 45, 234-242(DOI: 10.1016/j.expthermflusci.2012.11.014).

Chanson, H., Gualtieri, C. (2008). "Similitude and Scale Effects of Air Entrainment in Hydraulic Jumps." Journal of Hydraulic Research, IAHR, 46(1), 35-44.

Ead, S.A., Rajaratnam, N. (2002). "Hydraulic jumps on corrugated beds." J. Hydraul. Eng., 128(7), 656–663.

Felder, S. (2013). "Air-Water Flow Properties on Stepped Spillways for Embankment Dams: Aeration, Energy Dissipation and Turbulence on Uniform, Non-Uniform and Pooled Stepped Chutes." Ph.D. thesis, School of Civil Engineering, The University of Queensland, Brisbane, Australia .

Felder, S., Chanson, H. (2013). "Aeration, Flow Instabilities, and Residual Energy on Pooled Stepped Spillways of Embankment Dams." Journal of Irrigation and Drainage Engineering, 139(10), 880-887 (DOI: 10.1061/(ASCE)IR.1943-4774.0000627).

Felder, S., Chanson, H. (2014). "Air–water Flows and Free-surface Profiles on a Non-uniform Stepped Chute." Journal of Hydraulic Research, 52(2), 253-263 (DOI: 10.1080/00221686.2013.841780).

Felder, S., Chanson, H. (2015). "Phase-Detection Probe Measurements in High-Velocity Free-Surface Flows including a Discussion of Key Sampling Parameters." Experimental Thermal and Fluid Science, 61, 66-78 (DOI: 10.1016/j.expthermflusci.2014.10.009).

Felder, S., Chanson, H. (2016a). "An Experimental Study of Air-water Flows in Hydraulic Jumps with Channel Bed Roughness." WRL Research Report 259, UNSW Australia, Sydney, 166 pages.

Felder, S., Chanson H., (2016b). "Air-Water Flow in Hydraulic Jumps on Macro-Roughness", in Proc. of 20th Australasian Fluid Mechanics Conference, Perth, WA, 05 - 08 December, Paper 580, 4 pages.

Hager, W.H. (1992). "Energy Dissipators and Hydraulic Jump." Kluwer Academic Publishers, Water Science and Technology Library, Vol. 8, Dordrecht, the Netherlands, 288 pages.
Hughes, W.C., Flack, J.E. (1984). "Hydraulic jump properties over a rough bed." J. Hydraul. Eng., 110(12), 1755-1771.
Leng, X., Chanson, H. (2015). "Negative Surges and Unsteady Turbulent Mixing induced by Rapid Gate Opening in a Channel." Experimental Thermal and Fluid Science, 63, 133-143 (DOI: 10.1016/j.expthermflusci.2014.06.015).
Lennon, J.M., Hill, D.F. (2006). "Particle Image Velocimetry Measurements of Undular and Hydraulic Jumps." J. Hydraul. Eng., 132(12), 1283-1294.
Leutheusser, H.J., Schiller, E.J. (1975). "Hydraulic jump in a rough channel"; Int Water Power Dam Constr, 27(5), 186-191.
Lighthill, J. (1978). Waves in fluids, Cambridge University Press, Cambridge, UK.
Liu, M., Rajaratnam, N., Zhu, D.Z. (2004). "Turbulent Structure of Hydraulic Jumps of Low Froude Numbers." J. Hydraul. Eng., 130(6), 511-520.
Long, D., Rajaratnam, N., Steffler, P.M., Smy, P.R. (1991). "Structure of Flow in Hydraulic Jumps." Journal of Hydraulic Research, 29(2), 207-218.
Montes, J. S., Chanson, H. (1998). "Characteristics of Undular Hydraulic Jumps. Results and Calculations." J. Hydraul. Eng., 124(2), 192-205.
Mossa, M. (1999). "On the oscillating characteristics of hydraulic jumps" Journal of Hydraulic Research, 37(4), 541–558
Murzyn, F., Chanson, H. (2008). "Experimental Assessment of Scale Effects Affecting Two-Phase Flow Properties in Hydraulic Jumps." Experiments in Fluids, 45(3), 513-521 (DOI: 10.1007/s00348-008-0494-4).
Pagliara, S., Lotti, I., Palermo, M. (2008). "Hydraulic Jumps on Rough Bed of Stream Rehabilitation Structures. Journal of Hydro-Environment Research, 2(1), 29–38.
Pagliara, S., Palermo, M. (2015). "Hydraulic Jumps on Rough and Smooth Beds: Aggregate Approach for Horizontal and Adverse-sloped Beds" Journal of Hydraulic Research, 53(2), 243–252.
Rajaratnam, N. (1967). " Hydraulic Jumps." Advances in Hydroscience, Vol. 4, Ed. by V.T. Chow, Academic Press, N.Y., 197-280.
Rajaratnam, N. (1968). ''Hydraulic Jumps on Rough Beds'' Trans. Eng., Inst. Canada, 11, 1–8.
Reinauer, R., Hager, W.H. (1995) Non-breaking Undular Hydraulic Jump, Journal of Hydraulic Research, 33(5), 683-698.
Resch, F.J., Leutheusser, H.J. (1972). "Reynolds Stress Measurements in Hydraulic Jumps." Journal of Hydraulic Research. 10(4), 409-429.
Rouse, H., Siao, T.T., Nagaratnam, S. (1959). "Turbulence Characteristics of the Hydraulic Jump." Transactions. ASCE, 124, 926-950.
USBR (1987). "Design of Small Dams." Bureau of Reclamation, US Department of the Interior, Denver CO, USA, 3rd edition.
Wang, H. (2014). "Turbulence and Air Entrainment in Hydraulic Jumps." Ph.D. thesis, School of Civil Engineering, The University of Queensland, Brisbane, Australia, 341 pages & Digital appendices (DOI: 10.14264/uql.2014.542).
Wang, H., Chanson, H. (2015). "Experimental Study of Turbulent Fluctuations in Hydraulic Jumps." J. Hydraul. Eng., 141(7), Paper 04015010 10 pages (DOI: 10.1061/(ASCE)HY.1943-7900.0001010).
Wang, H., Felder, S., Chanson, H. (2014). "An Experimental Study of Turbulent Two-Phase Flow in Hydraulic Jumps and Application of a Triple Decomposition Technique." Experiments in Fluids, 55(7), Paper 1775, 18 pages & 2 video movies (DOI: 10.1007/s00348-014-1775-8).
Wood, I., Ackers, P., Loveless, J. (1983). "General Method for Critical Point on Spillways." J. Hydraul. Eng., 109(2), 308-312.
Wu, S., Rajaratnam, N. (1996). "Transition from Hydraulic Jump to Open Channel Flow." J. Hydraul. Eng., 122(9), 526-528.

FELDER, S., and CHANSON, H. (2018). "Air–Water Flow Patterns of Hydraulic Jumps on Uniform Beds Macroroughness." *Journal of Hydraulic Engineering*, ASCE, Vol. 144, No. 3, Paper 04017068, 12 pages (DOI: 10.1061/(ASCE)HY.1943-7900.0001402) (ISSN 0733-9429).

Zhang, W., Liu, M., Zhu, D., Rajaratnam, N. (2014). "Mean and Turbulent Bubble Velocities in Free Hydraulic Jumps for Small to Intermediate Froude Numbers." J. Hydraul. Eng., 140(11), paper 04014055.

Tables

Table 1. Experimental studies of hydraulic jumps with rough channel bed

Reference	k_s [mm]	Comment	B [m]	d_1 [mm]	Fr_1	Re	Q_w [m^3/s]	Instrumentation
Rajaratnam (1968)	1-2.5 9	Wire mesh & gravel	0.311	15.5-49	4.3-9.5	4×10^4-1.5×10^5	0.012-0.050	Point gauge, Pitot tube
Leutheusser and Schiller (1975)	5.6-22	Roughness spheres & strips	0.235	--	1-4	$1.5\text{-}5\times10^5$	-	Point gauge, Pitot tube
Hughes and Flack (1984)	3.2-11.3	Strip roughness & gravel	0.305	11-33	2.3-10.5	-	0.010-0.015	Point gauge
Ead and Rajaratnam (2002)	-	Corrugated sheet	0.446	25 & 51	4-10	5.1×10^5- 2.1×10^6	0.023-0.092	Point gauge, Pitot tube
Carollo et al. (2007)	4.6-32	Gravel	0.60	15-70	2.2-8.7	--	--	Point gauge
Pagliara et al. (2008)	6.7-45.6	Uniform & non-homogeneous gravel	0.35	0.99-34	2.2-12.2	2.2×10^4-1.1×10^5	0.006-0.031	Point gauge
Pagliara and Palermo (2015)	6.7-45.6	Gravel on inclined channel	0.345	--	2-9.5	--	--	Point gauge; single-tip conductivity probe
Present study	0.1	<u>Smooth bed</u>	0.5					Point gauge; dual-tip conductivity probe
		h = 36 mm		36	5.1	1.1×10^5	0.055	
	12	<u>Rough bed 1</u>						
		h = 20 mm		34-44	1.5-6.5	3.3×10^4-1.3×10^5	0.012-0.065	
		h = 36 mm		45-56	1.9-5.5	6.8×10^4-1.7×10^5	0.034-0.083	
		h = 52 mm		63-66	1.5-4.2	7.8×10^4-2.1×10^5	0.039-0.103	
	39	<u>Rough bed 2</u>						
		h = 20 mm		36-50	1.9-4.6	6.3×10^4-9.7×10^4	0.032-0.049	
		h = 36 mm		54-65	1.9-4.2	8.3×10^4-1.7×10^5	0.042-0.083	
		h = 52 mm		68-73	1.7-3.8	1.0×10^5-2.1×10^5	0.050-0.106	

FELDER, S., and CHANSON, H. (2018). "Air–Water Flow Patterns of Hydraulic Jumps on Uniform Beds Macroroughness." *Journal of Hydraulic Engineering*, ASCE, Vol. 144, No. 3, Paper 04017068, 12 pages (DOI: 10.1061/(ASCE)HY.1943-7900.0001402) (ISSN 0733-9429).

List of captions

Fig. 1. Experimental channel and bed roughness configurations
(A) Bed roughness 1; Note the header tank with sluice gate on the right-hand side of the figure
(B) Bed roughness 2; Note the sluice gate on the top of the figure

Fig. 2. Hydraulic jumps on bed roughness configuration 1
(A) Undular hydraulic jump: $Fr_1 = 2.1$; $Q_w = 0.053$ m^3/s; $Re = 1.0\times10^5$; h = 52 mm
(B) Undular hydraulic jump with air entrainment: $Fr_1 = 2.6$; $Q_w = 0.043$ m^3/s; $Re = 8.7\times10^4$; h = 36 mm
(C) Hydraulic jump with aerated jump toe: $Fr_1 = 2.8$; $Q_w = 0.031$ m^3/s; $Re = 6.3\times10^4$; h = 20 mm
(D) Hydraulic jump with stable jump toe roller: $Fr_1 = 4.5$; $Q_w = 0.085$ m^3/s; $Re = 1.7\times10^5$; h = 36 mm

Fig. 3. Comparison of jump toe perimeter characteristics on smooth and rough bed configuration 1: Smooth bed: $Fr_1 = 5.1$, $Re = 1.1 \times 10^5$, h = 36 mm; Rough bed 1: $Fr_1 = 6.5$, $Re = 1.3 \times 10^5$, h = 20 mm; Rough bed 1: $Fr_1 = 5.5$, $Re = 1.6 \times 10^5$, h = 36 mm; Rough bed 1: $Fr_1 = 4.2$, $Re = 2.0 \times 10^5$, h = 52 mm
(A) Average jump toe perimeter position
(B) Standard deviation of jump toe perimeter position
(C) Difference between 10th and 90th percentiles of jump toe perimeter positions

Fig. 4. Hydraulic jumps on bed roughness configuration 2
(A) Undular hydraulic jump with air entrainment: $Fr_1 = 2.1$; $Q_w = 0.032$ m^3/s; $Re = 6.3\times10^4$; h = 20 mm
(B) Hydraulic jump with standing wave and air entrainment: $Fr_1 = 2.9$; $Q_w = 0.082$ m^3/s; $Re = 1.6\times10^5$; h = 52 mm
(C) Oscillating jump between standing wave and roller jumps: $Fr_1 = 3.0$; $Q_w = 0.078$ m^3/s; $Re = 1.6\times10^5$; h = 36 mm
(D) Hydraulic jump with jump toe roller: $Fr_1 = 4.3$; $Q_w = 0.124$ m^3/s; $Re = 2.5\times10^5$; h = 52 mm

Fig. 5. Conjugate depth relationship for the rough channel bed configurations; Data include pointer gauge (PG) and air-water flow data; Comparison between experimental data, Bélanger equation (Eq. (3)) and $d_2/d_1 = Fr_1$ (Ead and Rajaratnam 2002)

Fig. 6. Dimensionless boundary friction force and average boundary shear stress in hydraulic jump over rough channel bed
(A) Boundary friction force
(B) Shear stress; Air-water flow data for d_1 only

Fig. 7. Comparison of basic air-water flow properties in hydraulic jumps with different bed roughness: Rough bed 1: $Fr_1 = 4.3$, $Re = 1.4 \times 10^5$, h = 36 mm; Rough bed 2: $Fr_1 = 4.2$, $Re = 1.7 \times 10^5$, h = 36 mm; Smooth bed: $Fr_1 = 5.1$, $Re = 1.1 \times 10^5$, h = 36 mm
(A) Void fraction distributions
(B) Bubble count rate distributions
(C) Interfacial velocity distributions

FELDER, S., and CHANSON, H. (2018). "Air–Water Flow Patterns of Hydraulic Jumps on Uniform Beds Macroroughness." *Journal of Hydraulic Engineering*, ASCE, Vol. 144, No. 3, Paper 04017068, 12 pages (DOI: 10.1061/(ASCE)HY.1943-7900.0001402) (ISSN 0733-9429).

Fig. 1. Experimental channel and bed roughness configurations
(A) Bed roughness 1; Note the header tank with sluice gate on the right-hand side of the figure

(B) Bed roughness 2; Note the sluice gate on the top of the figure

FELDER, S., and CHANSON, H. (2018). "Air–Water Flow Patterns of Hydraulic Jumps on Uniform Beds Macroroughness." *Journal of Hydraulic Engineering*, ASCE, Vol. 144, No. 3, Paper 04017068, 12 pages (DOI: 10.1061/(ASCE)HY.1943-7900.0001402) (ISSN 0733-9429).

Fig. 2. Hydraulic jumps on bed roughness configuration 1
(A) Undular hydraulic jump: $Fr_1 = 2.1$; $Q_w = 0.053$ m^3/s; $Re = 1.0\times10^5$; h = 52 mm

(B) Undular hydraulic jump with air entrainment: $Fr_1 = 2.6$; $Q_w = 0.043$ m^3/s; $Re = 8.7\times10^4$; h = 36 mm

(C) Hydraulic jump with aerated jump toe: $Fr_1 = 2.8$; $Q_w = 0.031$ m^3/s; $Re = 6.3\times10^4$; h = 20 mm

(D) Hydraulic jump with stable jump toe roller: $Fr_1 = 4.5$; $Q_w = 0.085$ m^3/s; $Re = 1.7\times10^5$; h = 36 mm

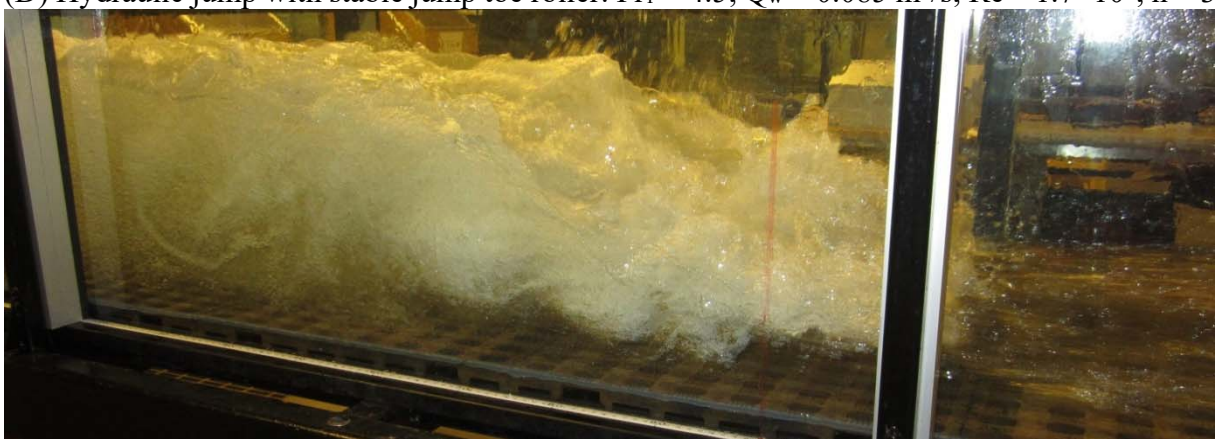

FELDER, S., and CHANSON, H. (2018). "Air–Water Flow Patterns of Hydraulic Jumps on Uniform Beds Macroroughness." *Journal of Hydraulic Engineering*, ASCE, Vol. 144, No. 3, Paper 04017068, 12 pages (DOI: 10.1061/(ASCE)HY.1943-7900.0001402) (ISSN 0733-9429).

Fig. 3. Comparison of jump toe perimeter characteristics on smooth and rough bed configuration 1: Smooth bed: Fr_1 = 5.1, Re = 1.1 × 10^5, h = 36 mm; Rough bed 1: Fr_1 = 6.5, Re = 1.3 × 10^5, h = 20 mm; Rough bed 1: Fr_1 = 5.5, Re = 1.6 × 10^5, h = 36 mm; Rough bed 1: Fr_1 = 4.2, Re = 2.0 × 10^5, h = 52 mm

(A) Average jump toe perimeter position

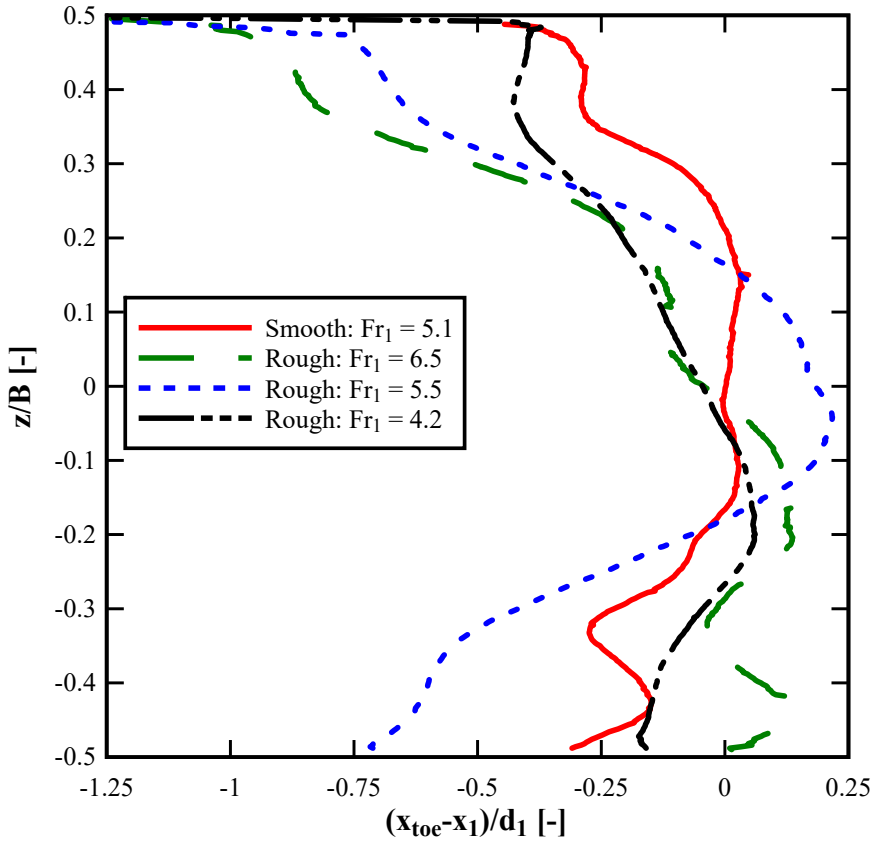

FELDER, S., and CHANSON, H. (2018). "Air–Water Flow Patterns of Hydraulic Jumps on Uniform Beds Macroroughness." *Journal of Hydraulic Engineering*, ASCE, Vol. 144, No. 3, Paper 04017068, 12 pages (DOI: 10.1061/(ASCE)HY.1943-7900.0001402) (ISSN 0733-9429).

Fig. 3. Comparison of jump toe perimeter characteristics on smooth and rough bed configuration 1: Smooth bed: Fr_1 = 5.1, Re = 1.1 × 10^5, h = 36 mm; Rough bed 1: Fr_1 = 6.5, Re = 1.3 × 10^5, h = 20 mm; Rough bed 1: Fr_1 = 5.5, Re = 1.6 × 10^5, h = 36 mm; Rough bed 1: Fr_1 = 4.2, Re = 2.0 × 10^5, h = 52 mm
(B) Standard deviation of jump toe perimeter position

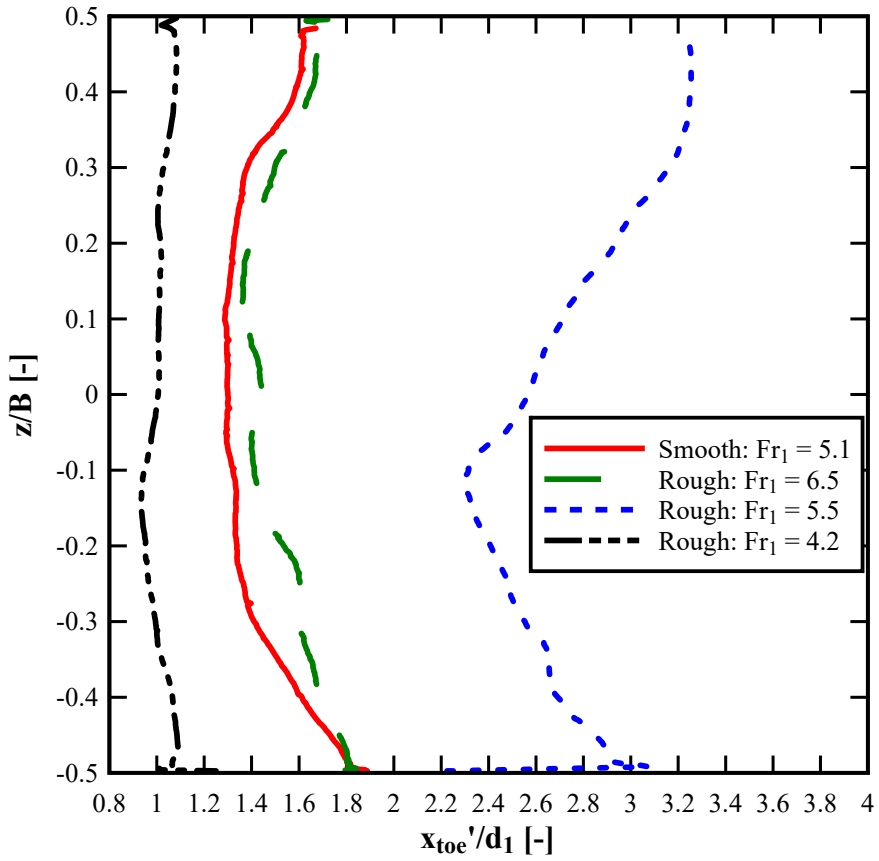

FELDER, S., and CHANSON, H. (2018). "Air–Water Flow Patterns of Hydraulic Jumps on Uniform Beds Macroroughness." *Journal of Hydraulic Engineering*, ASCE, Vol. 144, No. 3, Paper 04017068, 12 pages (DOI: 10.1061/(ASCE)HY.1943-7900.0001402) (ISSN 0733-9429).

Fig. 3. Comparison of jump toe perimeter characteristics on smooth and rough bed configuration 1: Smooth bed: Fr_1 = 5.1, Re = 1.1 × 10^5, h = 36 mm; Rough bed 1: Fr_1 = 6.5, Re = 1.3 × 10^5, h = 20 mm; Rough bed 1: Fr_1 = 5.5, Re = 1.6 × 10^5, h = 36 mm; Rough bed 1: Fr_1 = 4.2, Re = 2.0 × 10^5, h = 52 mm
(C) Difference between 10^{th} and 90^{th} percentiles of jump toe perimeter positions

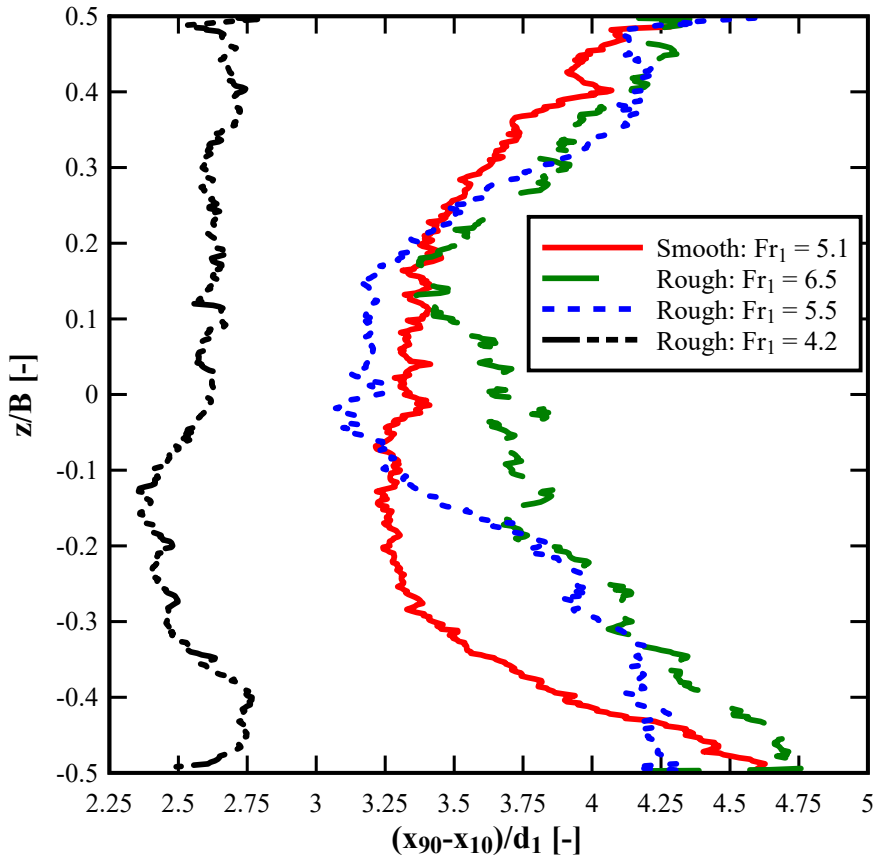

FELDER, S., and CHANSON, H. (2018). "Air–Water Flow Patterns of Hydraulic Jumps on Uniform Beds Macroroughness." *Journal of Hydraulic Engineering*, ASCE, Vol. 144, No. 3, Paper 04017068, 12 pages (DOI: 10.1061/(ASCE)HY.1943-7900.0001402) (ISSN 0733-9429).

Fig. 4. Hydraulic jumps on bed roughness configuration 2
(A) Undular hydraulic jump with air entrainment: $Fr_1 = 2.1$; $Q_w = 0.032$ m^3/s; $Re = 6.3\times10^4$; h = 20 mm

(B) Hydraulic jump with standing wave and air entrainment: $Fr_1 = 2.9$; $Q_w = 0.082$ m^3/s; $Re = 1.6\times10^5$; h = 52 mm

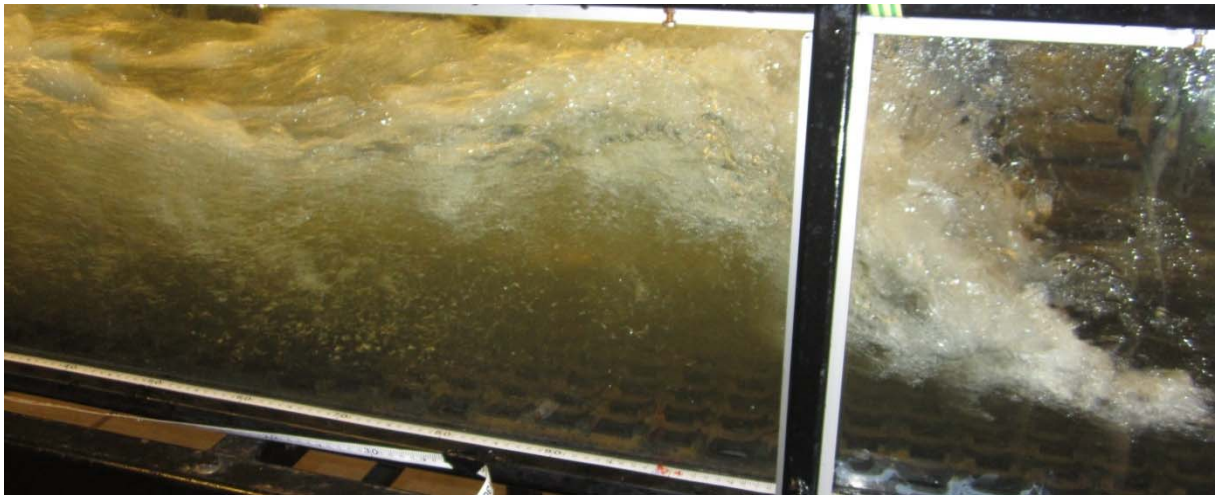

Fig. 4. Hydraulic jumps on bed roughness configuration 2
(C) Oscillating jump between standing wave and roller jumps: $Fr_1 = 3.0$; $Q_w = 0.078$ m^3/s; Re = 1.6×10^5; h = 36 mm

(D) Hydraulic jump with jump toe roller: $Fr_1 = 4.3$; $Q_w = 0.124$ m^3/s; Re = 2.5×10^5; h = 52 mm

Fig. 5. Conjugate depth relationship for the rough channel bed configurations; Data include pointer gauge (PG) and air-water flow data; Comparison between experimental data, Bélanger equation (Eq. (3)) and $d_2/d_1 = Fr_1$ (Ead and Rajaratnam 2002)

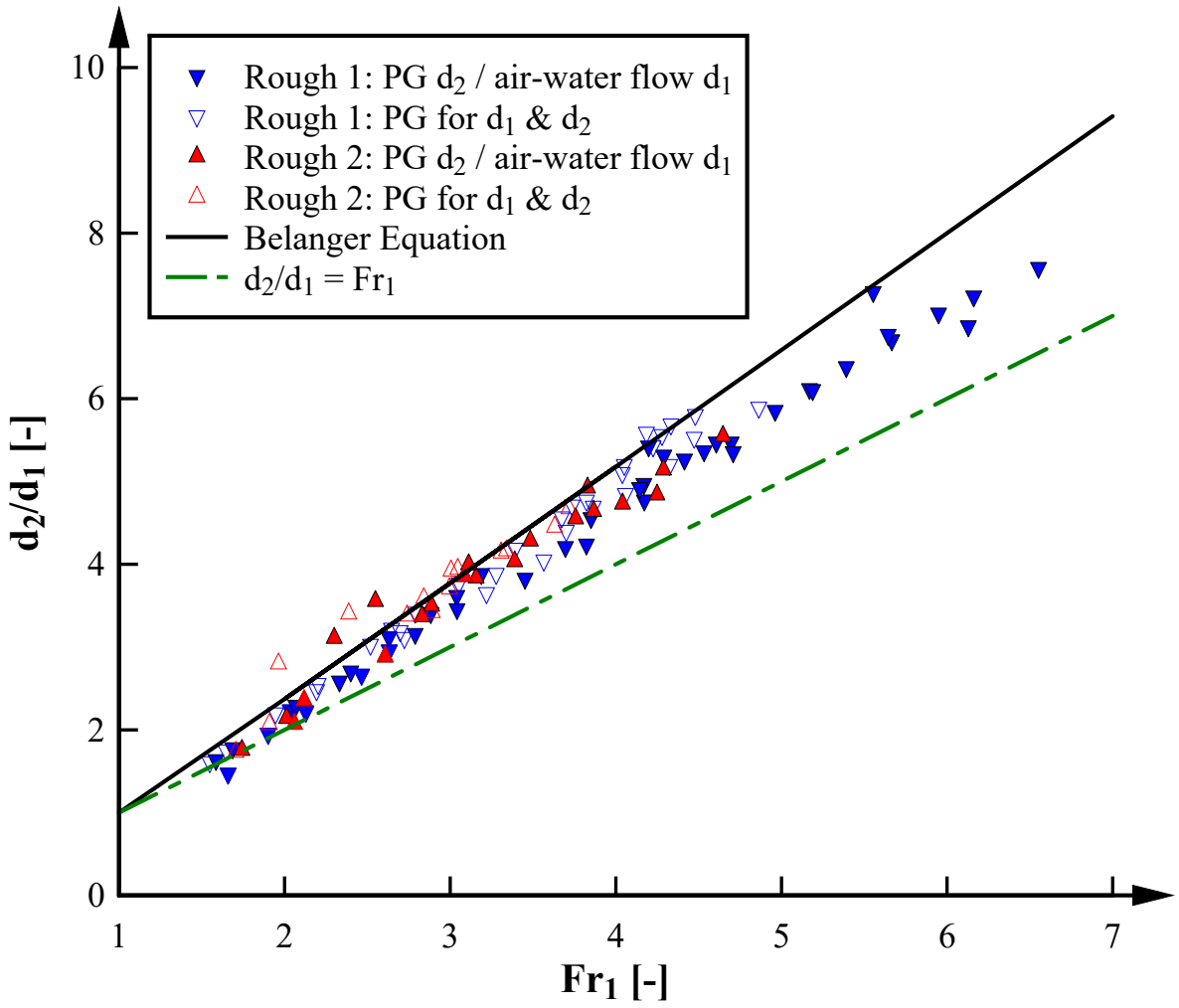

FELDER, S., and CHANSON, H. (2018). "Air–Water Flow Patterns of Hydraulic Jumps on Uniform Beds Macroroughness." *Journal of Hydraulic Engineering*, ASCE, Vol. 144, No. 3, Paper 04017068, 12 pages (DOI: 10.1061/(ASCE)HY.1943-7900.0001402) (ISSN 0733-9429).

Fig. 6. Dimensionless boundary friction force and average boundary shear stress in hydraulic jump over rough channel bed
(A) Boundary friction force

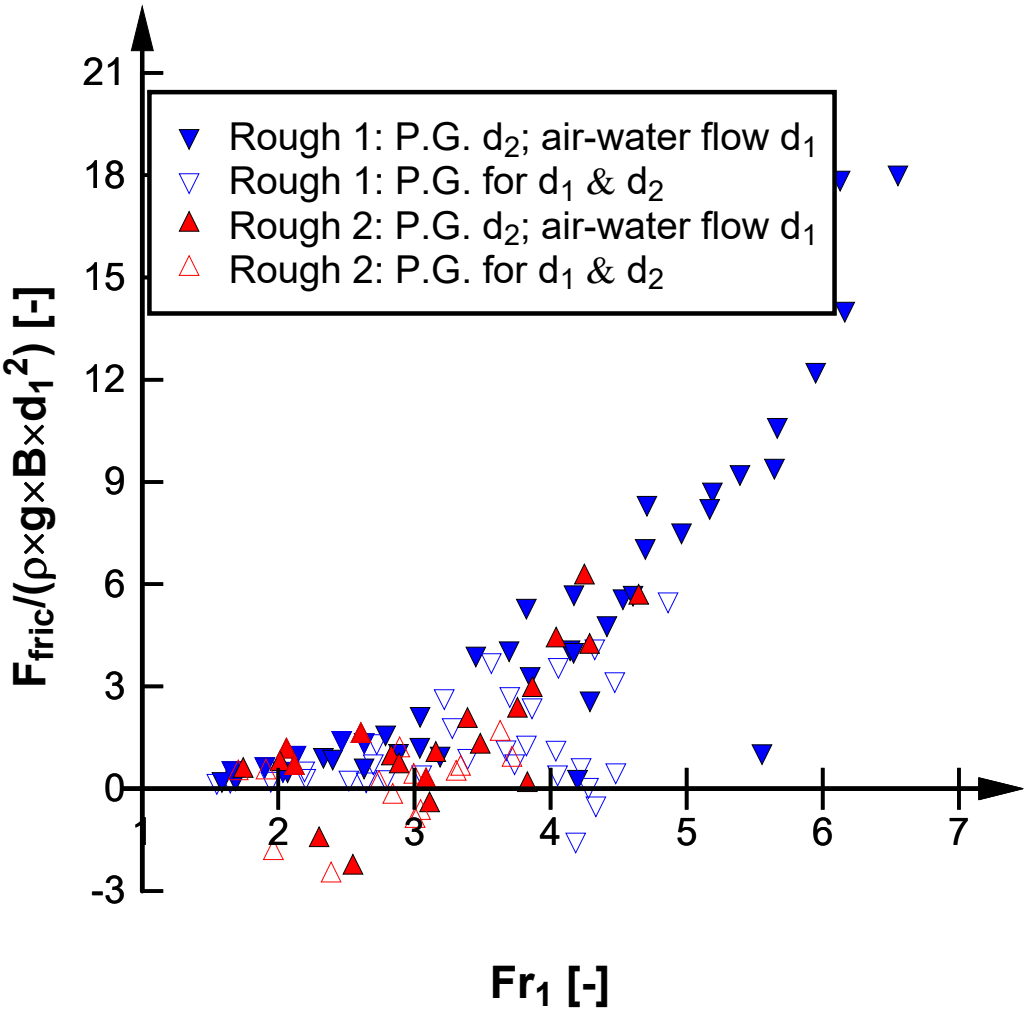

FELDER, S., and CHANSON, H. (2018). "Air–Water Flow Patterns of Hydraulic Jumps on Uniform Beds Macroroughness." *Journal of Hydraulic Engineering*, ASCE, Vol. 144, No. 3, Paper 04017068, 12 pages (DOI: 10.1061/(ASCE)HY.1943-7900.0001402) (ISSN 0733-9429).

Fig. 6. Dimensionless boundary friction force and average boundary shear stress in hydraulic jump over rough channel bed
(B) Shear stress; Air-water flow data for d_1 only

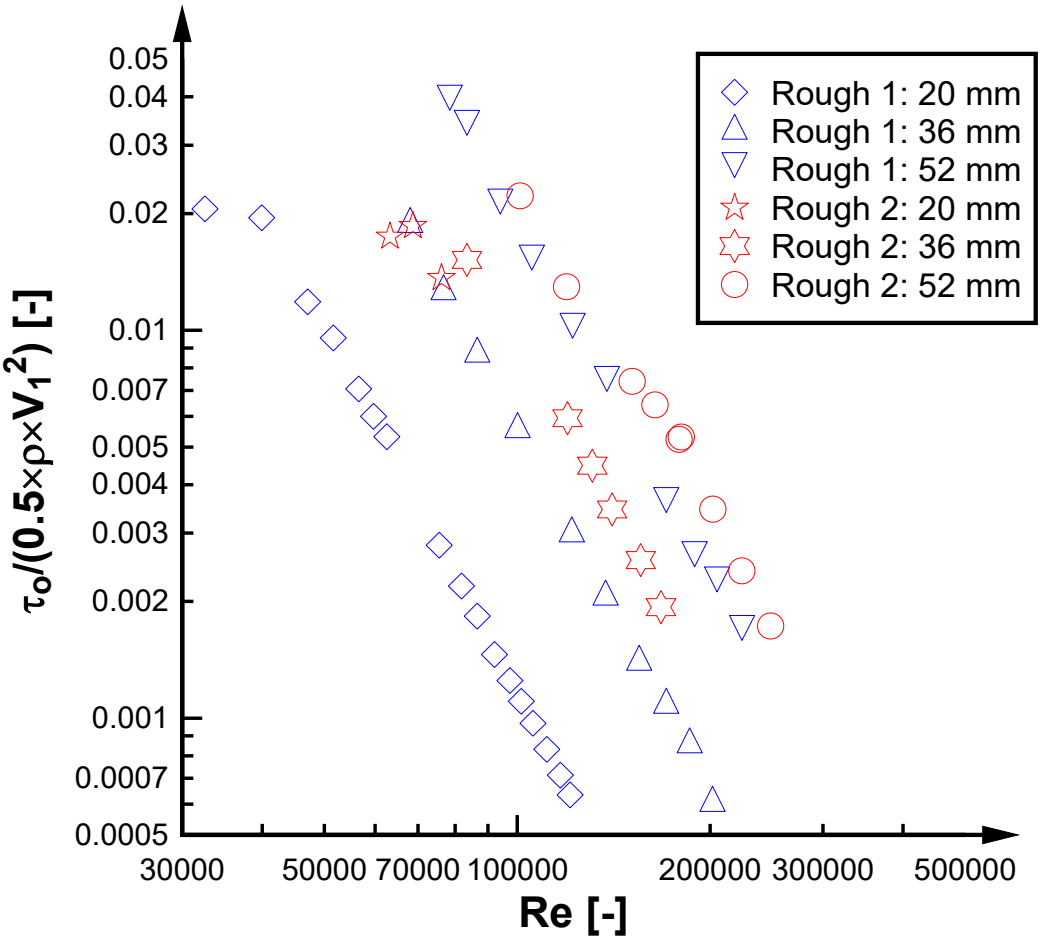

FELDER, S., and CHANSON, H. (2018). "Air–Water Flow Patterns of Hydraulic Jumps on Uniform Beds Macroroughness." *Journal of Hydraulic Engineering*, ASCE, Vol. 144, No. 3, Paper 04017068, 12 pages (DOI: 10.1061/(ASCE)HY.1943-7900.0001402) (ISSN 0733-9429).

Fig. 7. Comparison of basic air-water flow properties in hydraulic jumps with different bed roughness: Rough bed 1: Fr_1 = 4.3, Re = 1.4 × 10^5, h = 36 mm; Rough bed 2: Fr_1 = 4.2, Re = 1.7 × 10^5, h = 36 mm; Smooth bed: Fr_1 = 5.1, Re = 1.1 × 10^5, h = 36 mm
(A) Void fraction distributions

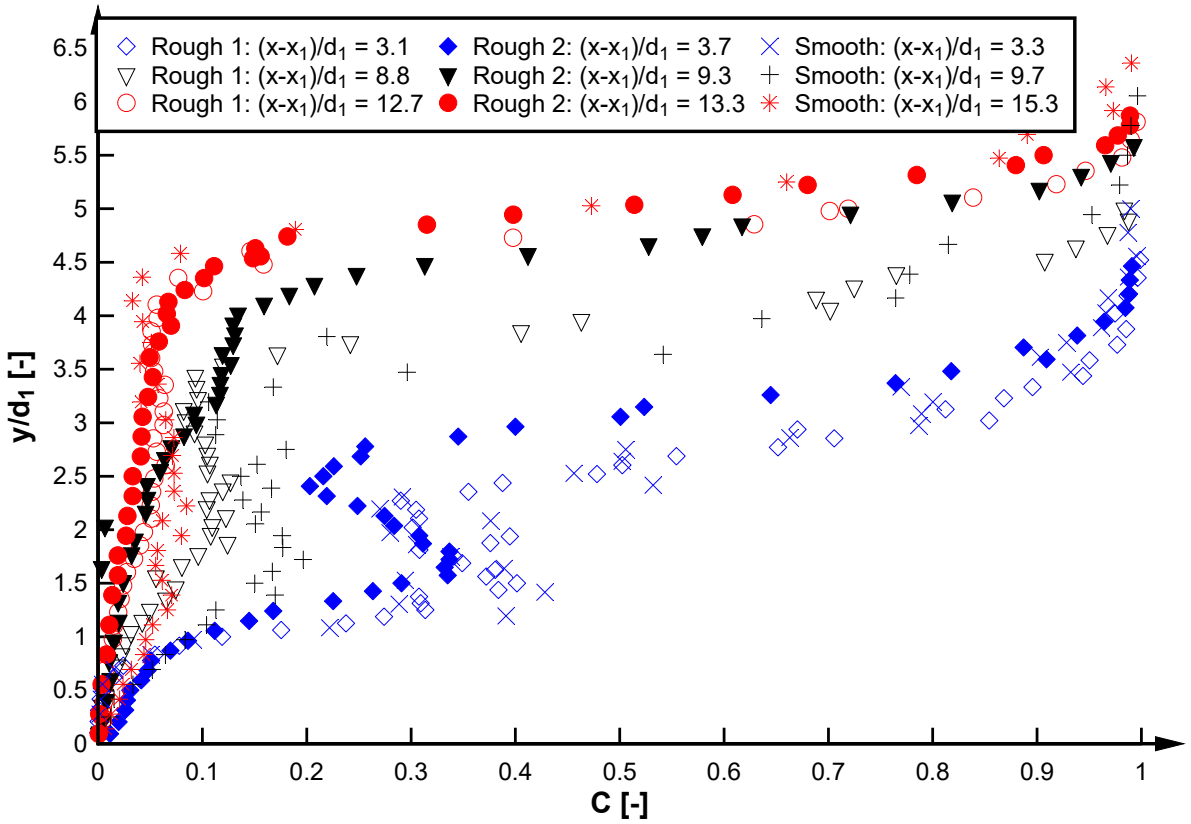

FELDER, S., and CHANSON, H. (2018). "Air–Water Flow Patterns of Hydraulic Jumps on Uniform Beds Macroroughness." *Journal of Hydraulic Engineering*, ASCE, Vol. 144, No. 3, Paper 04017068, 12 pages (DOI: 10.1061/(ASCE)HY.1943-7900.0001402) (ISSN 0733-9429).

Fig. 7. Comparison of basic air-water flow properties in hydraulic jumps with different bed roughness: Rough bed 1: Fr_1 = 4.3, Re = 1.4 × 10^5, h = 36 mm; Rough bed 2: Fr_1 = 4.2, Re = 1.7 × 10^5, h = 36 mm; Smooth bed: Fr_1 = 5.1, Re = 1.1 × 10^5, h = 36 mm
(B) Bubble count rate distributions

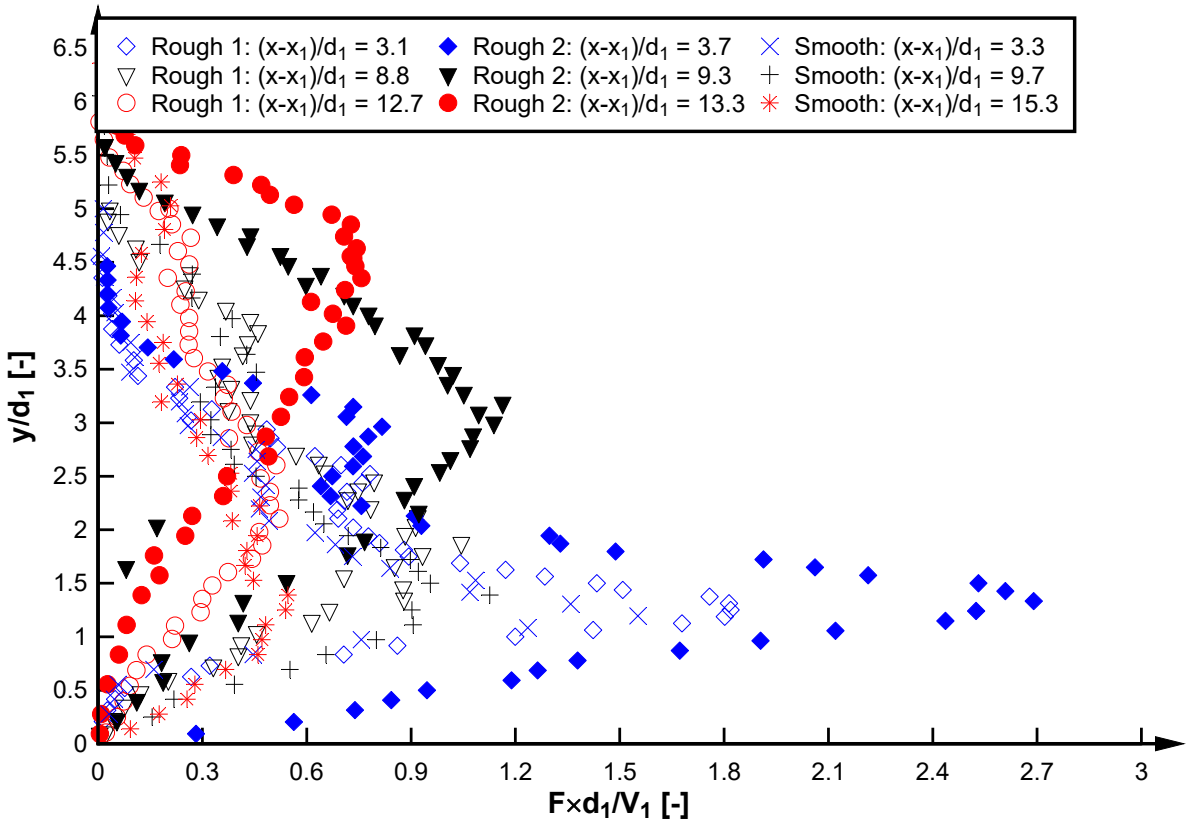

FELDER, S., and CHANSON, H. (2018). "Air–Water Flow Patterns of Hydraulic Jumps on Uniform Beds Macroroughness." *Journal of Hydraulic Engineering*, ASCE, Vol. 144, No. 3, Paper 04017068, 12 pages (DOI: 10.1061/(ASCE)HY.1943-7900.0001402) (ISSN 0733-9429).

Fig. 7. Comparison of basic air-water flow properties in hydraulic jumps with different bed roughness: Rough bed 1: Fr_1 = 4.3, Re = 1.4 × 10^5, h = 36 mm; Rough bed 2: Fr_1 = 4.2, Re = 1.7 × 10^5, h = 36 mm; Smooth bed: Fr_1 = 5.1, Re = 1.1 × 10^5, h = 36 mm
(C) Interfacial velocity distributions